Journal of Physics:
Conference Series

PAPER • **OPEN ACCESS**

Influence of thermal buoyancy on heat transfer in spacer-filled channels for Membrane Distillation

To cite this article: M Ciofalo *et al* 2025 *J. Phys.: Conf. Ser.* **2940** 012007

Journal of Physics: Conference Series **2940** (2025) 012007 doi:10.1088/1742-6596/2940/1/012007

Influence of thermal buoyancy on heat transfer in spacer-filled channels for Membrane Distillation

M Ciofalo, N Cancilla*, A Cipollina, A Tamburini and G Micale

Dipartimento di Ingegneria, Università degli Studi di Palermo, Viale delle Scienze Ed. 6, 90128 Palermo, Italy

* Corresponding author: nunzio.cancilla@unipa.it

Abstract. Numerical results are discussed for the flow in a horizontal plane channel filled with a novel sphere-rod spacer and exchanging heat from both the top and the bottom sides. Direct Numerical Simulations (DNS) are compared with RANS ones based on different turbulence models in the Reynolds number range 100~2000. Preliminary comparisons for non-buoyant flow show that models using wall functions perform poorly, grossly overpredicting Nusselt numbers, while ω-based models resolving the viscous-conductive sublayer all yield satisfactory results. In the presence of buoyancy, simulations using either DNS or the k-ω model yield a thermal asymmetry between top and bottom wall, confirmed by experiments and related to the stable or unstable thermal stratification occurring in the lower and upper layers of the channel. The asymmetry, large at low Re, becomes negligible for Re≥1000. The Spalart-Allmaras model yields satisfactory results in the absence of buoyancy but grossly overpredicts Nu in buoyant flows.

1. Introduction

In Membrane Distillation (MD) two fluids at different temperatures flow in two channels, feed (hot) and permeate (cold), separated by a hydrophobic membrane. The temperature difference between the fluids creates a trans-membrane vapour pressure difference among the channels, which is the driving force for the separation. The membrane allows the passage of vapour from the feed to the permeate, where it condenses, while rejecting the liquid and the non-volatile components (e.g., salts).

In MD, spacers are commonly employed both to support the membranes and to promote mixing, thus minimizing temperature polarization. Their optimum design requires a knowledge of the distribution of the local heat transfer coefficient and of its dependence on Reynolds number, spacer geometry and orientation between spacers and flow. In previous work [1,2,3] some of the present authors used a combination of experimental measurements (based on Thermochromic Liquid Crystals and digital image processing) and numerical simulations (including direct numerical simulations of turbulence) to study the distribution of the local heat transfer coefficient and the overall performances of different spacer configurations. Comparative results guided the choice of the best turbulence models in the Reynolds number range expected in MD (~200-2000) [4].

Recently, first Koutsou and Karabelas [5] and later Chong *et al.* [6] investigated by CFD a novel spacer geometry for mixing promotion (Figure 1). It consists of spheres connected by cylindrical rods so that the membrane-spacer contact is limited to isolated spots. Preliminary, TLC-based, experimental results were obtained for these spacers by some of the present authors [7].

Here, the results of direct numerical simulations (DNS) and RANS simulations using different turbulence models are presented for this spacer geometry under laminar to early turbulent flow conditions (Re≈100-2000). Two-side heat transfer is assumed. The influence of thermal buoyancy on heat transfer is also assessed.

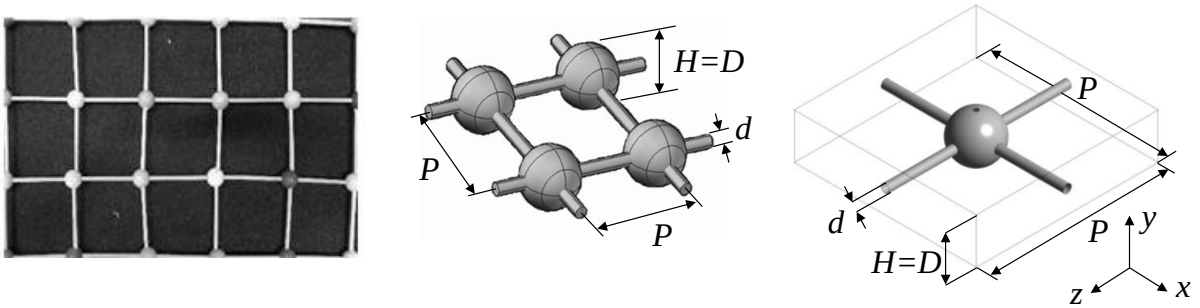

(a) (b) (c)

Figure 1. Sphere-rod spacers. (a) real spacer; (b) Sketch of the geometry; (c) computational domain. Nomenclature: H = channel height; D = sphere diameter; d = filament diameter; P = pitch.

2. Models and methods

2.1 Computational domain, governing equations and boundary conditions

The computational domain, representing the repetitive unit cell of a streamwise and spanwise indefinite array, is shown in Figure 1(c). The direction of the axes is indicated. The membranes are assumed to lie flat and horizontal, i.e. orthogonal to the gravity vector, as in the experiments [7].

Simulations were carried out under the assumption of fully developed flow and thermal field using the unit-cell approach, described in detail in previous work [2] ("Supplementary Material" section). The variables simulated were the velocity **u** and the periodic components p of pressure and T of temperature, so that translational periodicity could be imposed to the flow and thermal fields between opposite boundaries of the computational domains.

The governing equations were the continuity, momentum and energy ones for a Newtonian incompressible fluid with the Boussinesq approximation for buoyancy. In Cartesian tensor notation:

$$\frac{\partial u_j}{\partial x_j} = 0 \tag{1}$$

$$\frac{\partial \rho u_i}{\partial t} + \frac{\partial \rho u_j u_i}{\partial x_j} = -\frac{\partial p}{\partial x_i} + \frac{\partial}{\partial x_j}\mu\frac{\partial u_i}{\partial x_j} - \rho g_i \beta\left(T - T_0\right) + G_i \tag{2}$$

$$\frac{\partial \rho c_p T}{\partial t} + \frac{\partial \rho c_p u_j T}{\partial x_j} = \frac{\partial}{\partial x_j}\lambda\frac{\partial T}{\partial x_j} + S \tag{3}$$

where ρ, μ, λ and c_p are density, dynamic viscosity, thermal conductivity and specific heat; g_i is the i-th component of the gravity acceleration; β is the thermal expansion coefficient; T_0 is a reference temperature; G_i is a forcing term (driving pressure gradient) balancing the large-scale pressure loss; and S is a volumetric heat source term balancing the large-scale enthalpy loss from the hot fluid. A detailed analysis of the governing equations [2] shows that S must be expressed as $(\langle q''_w \rangle u_s)/(HU_s)$, in which $\langle q''_w \rangle$ is the area average of the heat flux q''_w exiting the channel from the walls, u_s is the local velocity component along the direction **s** of the forcing term $\mathbf{G}=\{G_i\}$, U_s is its average over the total volume (*superficial* velocity) and H is the channel height.

In the present simulations the **s** direction lay along the x axis. The forcing term G_i was imposed and dynamically adjusted so as to obtain a prescribed Reynolds number.

The no slip condition was imposed to the velocity field on all solid walls. In regard to thermal boundary conditions, the spacer surface was assumed to be adiabatic while on the upper and lower wall (simulating the membranes) Robin (third type) conditions were imposed:

$$T_w = T_c + r q''_w \tag{4}$$

where T_w is the wall temperature, T_c is the temperature of the external cold fluid (the condensate in a MD module) and r is an interposed thermal resistance, inclusive of the conductive resistance of the wall (membrane) and of the advective resistance on the cold channel side, supposed known.

The fluid properties were set to those of water at 39°C [9]. These values are immaterial once results are expressed in dimensionless form. Simulations were performed by the Ansys-CFX® code [8].

2.2 Main definitions

The Reynolds number Re is defined here as:

$$\mathrm{Re} = \frac{\rho U_s d_{eq}}{\mu} \tag{5}$$

where $d_{eq}=2H$ is the hydraulic diameter of the channel. The local Nusselt number Nu is defined as:

$$\mathrm{Nu} = \frac{q''_w}{\lambda\left(T_w - T_h\right)} \tag{6}$$

where T_h is the bulk temperature of the hot fluid. The mean Nusselt number $\langle \mathrm{Nu} \rangle$ is computed by substituting surface averages $\langle q''_w \rangle$ and $\langle T_w \rangle$ for q''_w and T_w. Partial averages can be computed over the top or the bottom wall to obtain the corresponding Nu.

2.3 Computational details

The most demanding case regards the direct numerical simulations (DNS). The Kolmogorov scale of the smallest energy carrying eddies is $\Lambda_K/H=(\nu^3/\varepsilon)^{1/4}$ in which ε is the rate of turbulence energy dissipation per unit mass and $\nu=\mu/\rho$ is the kinematic viscosity. In the present plane channel geometry, identifying ε with the total mechanical energy dissipation, it follows from the above definitions that:

$$\Lambda_K = 2.378\, f^{-1/4}\, \mathrm{Re}^{-3/4}\, H \tag{7}$$

where $f=|\mathbf{G}|(4H/\rho U_s^2)$ is the Darcy friction coefficient. For the highest Reynolds number simulated by DNS (Re≈2000), preliminary simulations indicate $f\approx 0.5$. Equation (7) yields $\Lambda_K \approx 10^{-2} H$. Therefore, an isotropic grid ($\Delta x=\Delta y=\Delta z=\Delta$) with 90 finite volumes along the cross-stream direction y and 360 along the x and z directions, yielding $\Delta/\Lambda_K \approx 1$, was judged adequate. The total number of the finite volumes was ~11.6 million. With this choice the viscous-conductive sublayer $y^+ \leq 11$ on the thermally active walls was resolved by ~10 volumes.

For the same case (DNS at Re≈2000) a time step of 10^{-3} s was adopted, corresponding to a RMS Courant number $\Delta t/(u\Delta x)$ of ~0.5. The simulations were protracted for 20 s, corresponding to ~30 wash-through times (P/U_s); the last 12 s were used to compute averages and statistics. The computing time was of the order of $1.3\cdot 10^5$ core-hours. The same Courant number and number of wash-through times were adopted at different Reynolds numbers. RANS simulations were run in steady-state mode with grids having from ~2.5 to ~6 million finite volumes. The symmetry properties of the geometry were not

exploited to simplify the computational domain. Based on previous computational experience [2,3], grid independence was amply satisfied in all cases.

2.4 Turbulence models

Most of the turbulence models which were compared can be grouped into families according to two criteria. The former criterion distinguishes first order eddy viscosity/eddy diffusivity models (*k*-ε [9], *k*-ω [11], BSL *k*-ω [12], SST [12]) from second order Reynolds stress/Reynolds flux models (LRR RS [13], SSG RS [14], ω RS [8]). The latter criterion distinguishes ω-based models, in which the viscous/conductive sublayer is explicitly resolved by the computational grid (*k*-ω, BSL *k*-ω, SST, ω RS) from *k*-based models, in which the sublayer is not explicitly resolved and wall functions are used (*k*-ε, LRR RS, SSG RS). A further model considered was the one-equation Spalart-Allmaras model [15] in which a transport equation for the eddy viscosity is solved. Space does not allow here a description of the above mentioned models, but they are all well documented in the cited references.

3. Results

3.1 Preliminary selection of turbulence models in the absence of buoyancy

Preliminarily, all models were compared with DNS for a Reynolds number of ~2000 in the absence of buoyancy (i.e., for β=0). Results are summarized in Figure 2, which shows maps of the local Nusselt number. The mean Nusselt number over a wall (indifferently top or bottom) is indicated.

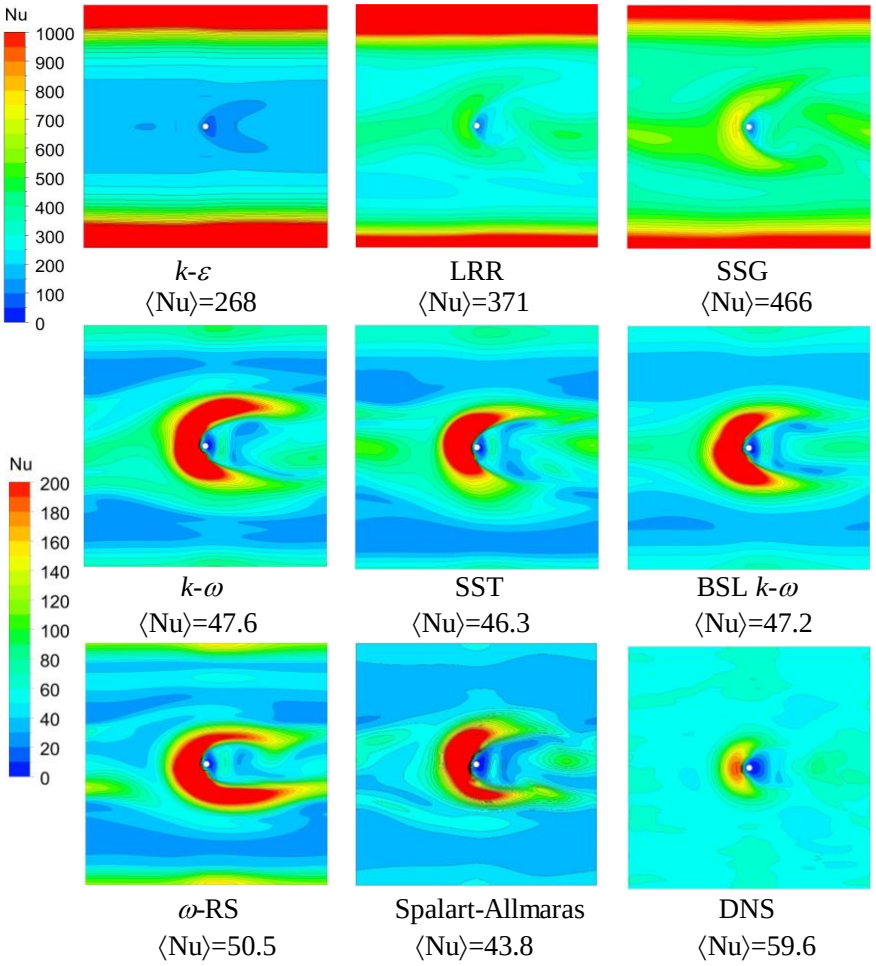

Figure 2. Nusselt number distributions over one of the walls for the nine models tested (Re≈2000, no buoyancy, flow from left to right). DNS results are time averaged.

It is clear from these results that models using wall functions, either of first (k-ε) or of second order (LRR, SSG), are totally inadequate: they overpredict ⟨Nu⟩ by 4-8 times with respect to DNS and yield a wrong distribution of the local Nusselt number. All ω-based models resolving the viscous-conductive sublayer yield acceptable and very similar results, with computed values of ⟨Nu⟩ from 78% to 85% of the DNS prediction. Even the one-equation Spalart-Allmaras model yields a satisfactory value of ⟨Nu⟩, only slightly below the ω-based models, and a similar spatial distribution of Nu.

3.2 Influence of thermal buoyancy

On the basis of the above comparisons, all following simulations were limited to three models: DNS, k-ω (representative, with only ±4% differences in ⟨Nu⟩ and utterly negligible differences in flow quantities, of all ω-based models) and Spalart-Allmaras (as a one-of-a-kind, eddy viscosity transport-based, model). All subsequent simulations were performed with buoyancy on, with the explicit purpose of assessing the influence of natural convection on heat transfer coefficients and its dependence on the Reynolds number in a spacer-filled channel geometry.

Note that, in a simple "void" (i.e., spacerless) horizontal plane channel, thermal buoyancy causes an asymmetry between the Nu distributions on the top and bottom walls even in the presence of perfectly symmetrical thermal boundary conditions. This is illustrated in Figure 3. Graph (a) is a sketch of the temperature distribution across a hot channel surrounded by two identical cold channels, as occurs in direct contact membrane distillation (DCMD) stacks and in the test section used in the most recent of our experiments [7]. Stable thermal stratification $\partial T/\partial y>0$ (expected to be associated with laminarized flow and low heat transfer rates) will occur in the bottom half of the hot channel, unstable stratification $\partial T/\partial y<0$ (expected to be associated with buoyancy-promoted turbulence and high heat transfer rates) in the top half. Graph (b) is a plot of the experimentally measured ⟨Nu⟩ on the top and bottom walls as functions of Re for a temperature difference of ~20°C between the hot and cold channels [7]. Consistently with the above remarks on thermal stratification, $\langle Nu\rangle_{top}$ largely exceeds $\langle Nu\rangle_{bottom}$ at low Re, while the two values become almost identical for Re>~1000.

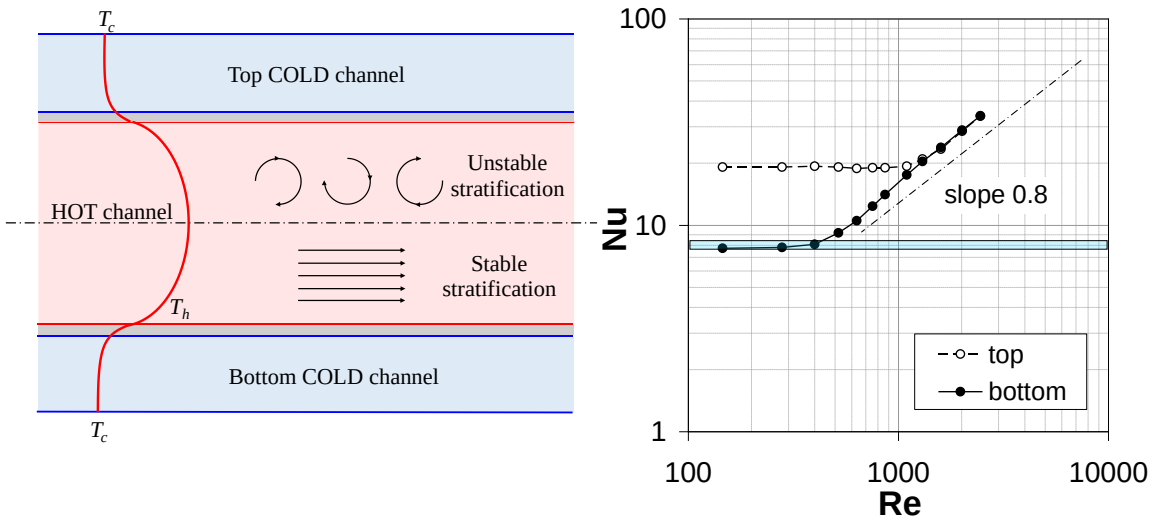

(a) (b)

Figure 3. Influence of buoyancy in a "void" (spacerless) horizontal plane channel. (a) Sketch of the temperature distribution across the channel, showing stable and unstable thermal stratification regions; (b) experimental ⟨Nu⟩ on the top and bottom wall as a function of Re.

An *a priori* estimate of the importance of buoyancy can be made on the basis of the Richardson number $Ri=Ra/Re^2$. Here, Re is the Reynolds number as defined by Eq. (5). Ra is the Rayleigh number

which, for the configuration in Figure 3(a), can be computed for a length scale $H/2$ as:

$$\mathrm{Ra} = \frac{g\beta\left(T_h - T_w\right)(H/2)^3}{\nu\alpha} \tag{8}$$

where $\alpha=\lambda/\rho c_p$ is the thermal diffusivity of the fluid. Taking account of the thermal boundary condition in Eq. (4) and of the definition of Nu in Eq. (6), the temperature difference T_h-T_w can be expressed as $a/(1+b\mathrm{Nu})$, with the constants a and b depending on the values chosen for r and T_c in Eq. (4). A common criterion is that heat transfer is dominated by buoyancy for Ri>~0.25.

Identifying Nu with $\langle \mathrm{Nu} \rangle_{top}$ as computed by the k-ω model, the behaviour of Ri as a function of Re is that shown in Figure 4.

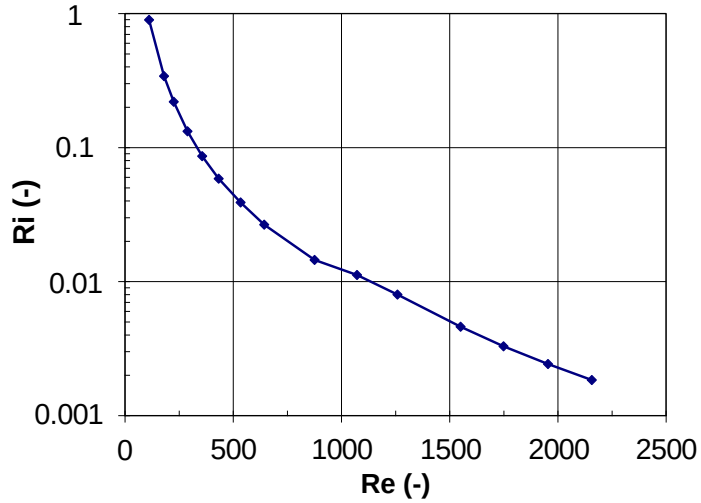

Figure 4. Richardson number as a function of the Reynolds number for a sphere-rod spacer-filled channel.

It can be observed that Ri is almost 1 at the lowest Re investigated (~100) but decreases rapidly with Re and becomes utterly negligible at Re>~1000. Therefore, one may expect the influence of buoyancy to be significant only at low Reynolds number, especially Re<300, and to practically vanish for Re>1000. The void-channel results in Figure 3(b) confirm this estimate.

Considering now spacer-filled channels, mean Nusselt numbers on the top and the bottom wall predicted by different turbulence models are reported in Figure 5 as functions of the Reynolds number. Experimental results in [7] are also shown.

DNS results behave like the experimental data for a void channel reported in Figure 3(b): $\langle \mathrm{Nu} \rangle_{top}$ largely exceeds $\langle \mathrm{Nu} \rangle_{bottom}$ at low Re, while the two values practically coincide and exhibit a roughly 0.8 power-law trend for Re≥~1000. The k-ω model (used here with buoyancy-related turbulence production terms activated in the k-transport equation but turned off in the ω-transport equation, as suggested in [16]) behaves similarly to DNS, although top and bottom $\langle \mathrm{Nu} \rangle$ values do not quite collapse on a single trend (as in DNS) up to Re≈4000. In the presence of buoyancy, the Spalart-Allmaras models becomes grossly inadequate, overpredicting $\langle \mathrm{Nu} \rangle$ by 6-20 times with respect to DNS on *both* walls.

Experimental results in [7] are qualitatively similar to DNS predictions, in that $\langle \mathrm{Nu} \rangle_{top}$ exceeds $\langle \mathrm{Nu} \rangle_{bottom}$ at low Re, while the two values become practically coincident for Re≥~1000. However, the experimental top-bottom asymmetry is lower than that exhibited by both DNS and k-ω predictions; more precisely, experimental, DNS and k-ω results are very close to one another on the bottom wall, but differ significantly on the top wall. A careful analysis of the differences between the experimental setup and the computational assumptions evidences that in the experiments the fluid enters the test section with

significant inlet turbulence levels, caused by the upstream circuit including expansions and direction changes. On the contrary, all simulations are conducted for fully developed flow and thermal conditions, and turbulence levels are the equilibrium ones between production (by shear, obstacles and buoyancy) and dissipation. Further investigations will be necessary to clarify this issue.

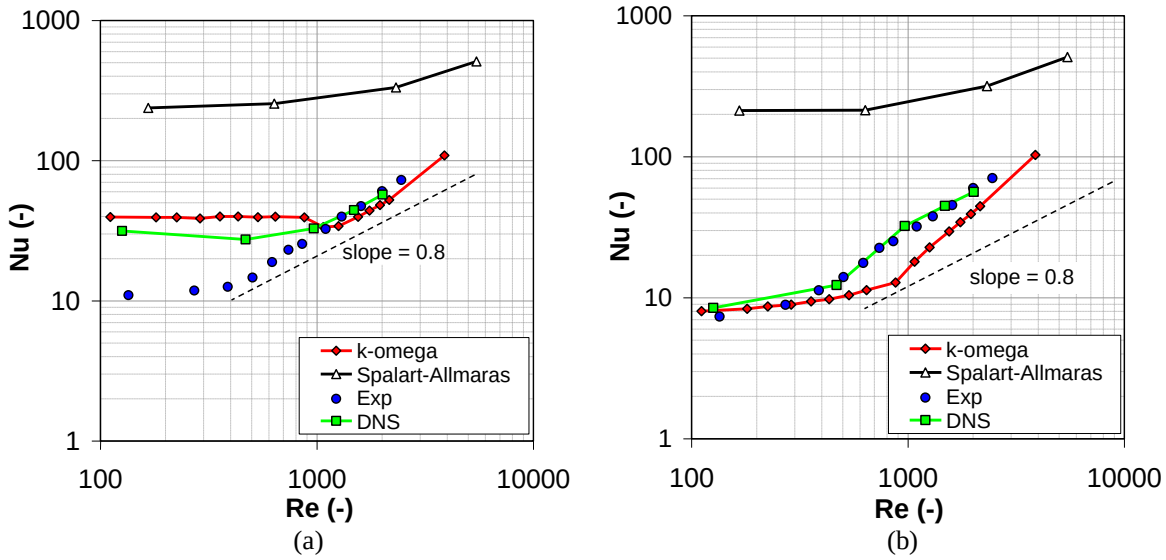

Figure 5. ⟨Nu⟩ as a function of Re for the sphere-rod spacer geometry of Figure 1 and different turbulence models. Experimental results [7] are also reported. (a) Top wall; (b) bottom wall.

Figure 6 reports maps of the turbulent kinetic energy k (a, c) and of the time-averaged temperature (b, d) in the mid xy plane predicted by DNS for Re≈130 (a, b) and Re≈1000 (c, d).

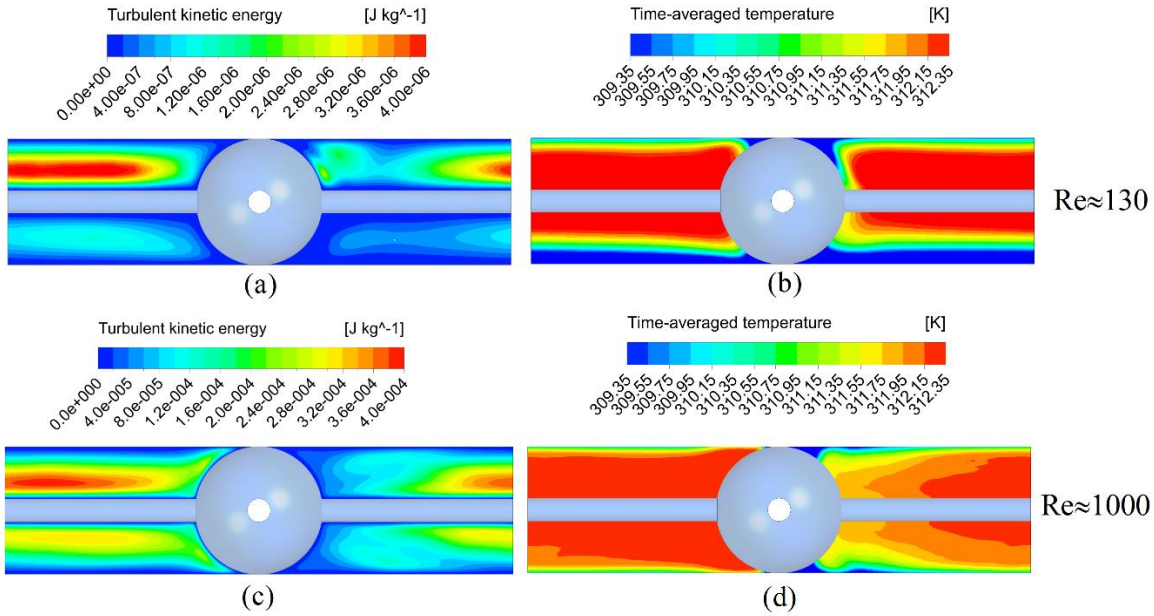

Figure 6. Turbulent kinetic energy k (a, c) and time-averaged temperature (b, d) in the mid xy plane predicted by DNS. (a, b) Re≈130; (c, d) Re≈1000. Flow is from left to right.

Consistently with the previous remarks on the Richardson number, the top-bottom asymmetry of both the k and the T distributions is much higher at the lower Reynolds number (Ri≈0.7), while it

becomes barely noticeable at the higher Re (Ri≈0.01). Notably, values of k, once scaled by Re^2 (i.e., by U_s^2) are similar in the two cases, indicating that turbulence is sustained even at a Reynolds number as low as ~130 thanks to the contribution of production by buoyancy (which is almost independent of Re).

4. Conclusions

Numerical results were obtained for buoyant and non-buoyant flow in a horizontal plane channel filled with a novel sphere-rod spacer and exchanging heat from both the top and the bottom sides, representative of membrane distillation units.

Preliminary simulations were conducted setting buoyancy off. In this case, in comparison with Direct Numerical Simulations, RANS models of both first and second order using wall functions (k-ε, SSG RS, LRR RS) performed poorly, grossly overpredicting Nusselt numbers, while ω-based models resolving the viscous-conductive sublayer (k-ω, BSL k-ω, SST, ω RS) all yielded satisfactory results with small differences between specific models.

In the presence of buoyancy, DNS runs predicted significant turbulence levels, sustained by buoyancy production, even at very low Reynolds numbers (e.g. ~100). ω-based RANS models failed to predict turbulence at Re<~1000, yielding instead velocity fluctuations in the iteration space, which are unphysical in steady-state simulations. Both DNS and k-ω simulations yielded a thermal asymmetry between top and bottom wall, confirmed also by experimental results for both spacerless and spacer-filled channels. This asymmetry is explained by the stable or unstable thermal stratification occurring in the lower and upper layers of the channel, respectively; it is large at low Re but becomes negligible for Re>~1000, consistently with estimates based on the Richardson number.

The Spalart-Allmaras eddy viscosity transport model exhibited an anomalous behaviour, yielding satisfactory results in the absence of buoyancy but a gross overprediction of Nusselt numbers in buoyant flows.

5. References

[1] Tamburini A, Pitò P, Cipollina A, Micale G and Ciofalo M 2013 *J. Membr. Sci.* **447** 260
[2] Tamburini A, Renda M, Cipollina A, Micale G and Ciofalo M 2016 *Int. J. Heat Mass Transf.* **93** 1190
[3] Ponzio F N, Tamburini A, Cipollina A, Micale G and Ciofalo M 2017 *Int. J. Heat Mass Transf.* **104** 163
[4] Ciofalo M, Di Liberto M, La Cerva M and Tamburini A 2019 *Int. J. Therm. Sci.* **145** 106040
[5] Koutsou C P and Karabelas A J 2015 *J. Memb. Sci.* **488** 129
[6] Chong Y K, Liang Y Y, Lau W J and Fimbres Weihs G A 2022 *Int. J. Heat Mass Transf.* **191** 122819
[7] Cancilla N, Tamburini A, Tarantino A, Visconti S and Ciofalo M 2022 *Membranes* **12** 1029
[8] ANSYS 2018 *ANSYS-CFX Reference Guide Release 18.2*
[9] Launder B E and Spalding D B 1974 *Comput. Methods Appl. Mech. Eng.* **3** 269
[10] Yakhot V, Orszag S A, Thangam S, Gatski T B and Speziale C G 1992 *Phys. Fluids A* **4** 1510
[11] Wilcox D C 1988 *AIAA J.* **26** 1299
[12] Menter F R 1994 *AIAA J.* **32** 1598
[13] Launder B E, Reece G J and Rodi W 1975 *J. Fluid Mech.* **68** 537
[14] Speziale C G, Sarkar S and Gatski T B 1991 *J. Fluid Mech.* **277** 245
[15] Spalart P R and Allmaras S R 1994 *La Recherche Aérospatiale* **1** 5
[16] Ciofalo M 2021 *Thermofluid Dynamics of Turbulent Flows – Fundamentals and Modelling* Springer, UNIPA-Springer Series

Acknowledgments

This work was partly performed within the Sol2H2O project (European Twinning for research in Solar Energy to Water Production and Treatment Technologies), funded by European Union under Horizon Europe research & innovation programme, grant agreement No: 101079305.